Six-year mercury dry deposition across North America

Leiming Zhang[1,*], Zhiyong Wu[1], Irene Cheng[1], L. Paige Wright[2], Mark L. Olson[3], David A. Gay[3], Martin R. Risch[4], Steven Brooks[5], Mark S. Castro[6], Gary D. Conley[7], Eric S. Edgerton[8], Thomas M. Holsen[9], Winston Luke[10], Robert Tordon[11], Peter Weiss-Penzias[12]

[1] Environment and Climate Change Canada, Toronto, ON
[2] Independent Researcher, Stratford, PEI
[3] University of Illinois, Champaign, IL
[4] U.S. Geological Survey; Indianapolis, IN
[5] The University of Tennessee Space Institute, Tullahoma, TN
[6] University of Maryland, Frostburg, MD
[7] GreenReach LLC, Glouster, OH
8 Atmospheric Research and Analysis, Durham, NC
[9] Clarkson University, Potsdam, NY
[10] NOAA Air Resources Laboratory, College Park, MD
[11] Environment and Climate Change Canada, Dartmouth, NS
[12] University of California, Santa Cruz, CA

Corresponds to: leiming.zhang@canada.ca

Abstract: Dry deposition of atmospheric mercury (Hg) to various land covers surrounding 24 sites in North America was estimated for the years 2009 to 2014. Depending on location, multi-year mean annual Hg dry deposition was estimated to range from 5.1 to 23.8 μg m^{-2} yr^{-1} to forested canopies, 2.6 to 20.8 μg m^{-2} yr^{-1} to non-forest vegetated canopies, 2.4 to 11.2 μg m^{-2} yr^{-1} to urban and built up land covers, and 1.0 to 3.2 μg m^{-2} yr^{-1} to water surfaces. In the rural or remote environment in North America, annual Hg dry deposition to vegetated surfaces is dominated by leaf uptake of gaseous elemental mercury (GEM), contrary to what was commonly assumed in earlier studies which frequently omitted GEM dry deposition as an important process. Dry deposition exceeded wet deposition by a large margin in all of the seasons except in the summer at the majority of the sites. GEM dry deposition over vegetated surfaces will not decrease at the same pace, and sometimes may even increase with decreasing anthropogenic emissions, suggesting that Hg emission reductions should be a long-term policy sustained by global cooperation.

Introduction: Mercury (Hg) released into the atmosphere from natural and anthropogenic sources will eventually return back to the soil and water surfaces through dry and wet deposition processes[1,2,3,4]. Excessive atmospheric Hg deposition results in enrichment of Hg in the biosphere which in turn causes detrimental effects on ecosystems, wildlife and human health[5,6]. Mitigation of these detrimental human health effects by adopting the Minamata Convention and domestic Hg control policies from the U.S. are predicted to lead to enormous economic benefits of up to hundreds of billions of dollars by 2050[7]. The National Atmospheric Deposition Program (NADP) Atmospheric Mercury Network (AMNet) was established in 2009 to monitor the three operationally-defined Hg forms in the atmosphere, i.e., GEM, gaseous oxidized mercury (GOM), and particulate-bound mercury (PBM) for subsequent Hg dry deposition estimation[8]. To meet this goal, a dry deposition framework has recently been developed[9,10,11], and is applied to the first six years of data in this study. Geographical and temporal patterns of Hg dry deposition over dominant land covers, relative contributions from the three forms of Hg to total dry deposition, and the relative importance of dry and wet deposition are discussed in detail. Uncertainty analyses are conducted to ensure the reliability of the estimated dry deposition. Responses of mercury dry deposition to future emission reductions from anthropogenic sources are assessed through sensitivity tests. Results presented in this study provide the much needed information for assessing the impact of atmospheric Hg on ecosystem health.

Sites description

Data at 24 sites are analyzed in this study (Table 1). Collocated instruments are deployed at three sites: MD98/MD99, MS12/MS99, and NY43/NY95. The sites are located in western and southern U.S., the Midwest, and northeastern North America (Fig. 1). The majority of the sites are located in the southern and northeastern regions and are rural sites. There are also three urban and seven suburban locations. Existing land cover in the vicinity (a 3 km radius circle) of the sampling site, which are used in the Hg dry deposition calculations, are also provided in Table 1 with more details provided in Sect. 2 of the Supplemental Information (SI). Hg air emissions, including point sources and fugitive air emissions within a 100 km radius of each site, are extracted from USEPA[12] and are listed in Table 1 and shown in Fig. 1.

Air concentrations

Speciated atmospheric Hg concentrations from 2009 to 2014 are used in this study[13]. Available measurement periods and multi-year mean values are listed in Table 1. Data collection, quality control procedures and statistics of multi-hourly concentrations are described in detail in Sect. 3 of the SI[8]. It should be noted that oxidized Hg collected using this instrument was likely biased low, as shown in Gustin et al.[14], and further discussed below.

The hourly GEM concentrations during 2009-2014 ranged from 0.2 to 258 ng m^{-3}, with the highest single observation observed at AL19. The multi-year mean GEM was generally the highest at urban sites (1.63 to 1.98 ng m^{-3} at NY06, UT97, and AL19), followed by suburban sites (1.45 to 1.65 ng m^{-3} at NJ05, CA48, NY43/95, ME97, and UT96) and rural locations (1.28 to 1.46 ng m^{-3} at most sites except 1.8 ng m^{-3} at OH52) (Table 1). Sites impacted by the marine boundary layer generally had low mean GEM (1.33 to 1.48 ng m^{-3} at NS01, NH06, MS99/12, and CA48). Mean GEM was the highest during winter and/or spring at the majority of the sites, and the lowest during the fall. There were also seven sites with higher mean GEM during the summer.

The 2-4 hourly concentrations ranged from 0 to 7700 pg m^{-3} for GOM and 0 to 7100 pg m^{-3} for PBM during 2009-2014, with the maxima of GOM and PBM recorded at the collocated MD98 and MD99 sites. The multi-year mean oxidized Hg (GOM+PBM) ranged from 4.1 to 17.6 pg m^{-3} among 21 sites, whereas it was 28.9 pg m^{-3} at AL19, 36.5 pg m^{-3} at UT97, and 215.5 pg m^{-3} at HI00. Excluding HI00, the multi-year mean GOM ranged from 0.36 to 20.4 pg m^{-3}, and PBM, from 0.43 to 16.1 pg m^{-3}, among 23 sites. The mean oxidized Hg at HI00 was nearly 20 times the average of the other 23 sites. The much higher oxidized Hg at this site was likely due to its high-elevation (3.4 km above sea level), and thus frequent impaction by the free troposphere, which can transport GOM and PBM from the upper atmosphere[15,16,17,18]. The relatively higher oxidized Hg at UT97 was likely due to a combination of these factors including urban site category, high elevation at 1.1 km, and very dry environment. A similar case to UT97 was found at UT96, which is a suburban site in western U.S. at an elevation of 1.3 km; Mean GOM at UT96 was 11.7 pg m^{-3}, ranked only after UT97 among all of the sites (note that there were not enough PBM data at UT96 to properly evaluate this site). The higher oxidized Hg at AL19 than at the other urban, suburban or rural sites was due to the very high Hg emissions in its vicinity (Table 1). Excluding HI00, urban sites had higher oxidized Hg (15.3 to 36.5 pg m^{-3} at NY06, Al19, and UT97) than suburban (4.1 to 16.9 pg m^{-3}) and rural (4.7 to 17.6 pg m^{-3}) sites. Most of the sites impacted by the marine boundary layer had low oxidized Hg (4.1 to 6.0 pg m^{-3} at CA48, NS01, and NH06, and 12.3 pg m^{-3} at MS99/12).

At the majority of the sites, the highest mean GOM was found in the spring (Fig. SI-4 in Sect. 3 of SI). There were five locations with higher mean GOM during the summer. The lowest mean GOM for most of the sites occurred either in the winter or summer. This is in contrast to PBM, in which the highest average concentrations were found during the winter for most of the sites. Higher average PBM during the spring were observed at four locations. The lowest average PBM at the majority of the sites occurred during the summer and fall.

Temporal trends in Hg from 2009-2014 were analyzed for the sites with six complete years of data. Although Hg emissions from local emission sources have declined year-after-year between 2009 and 2013 and remained almost constant from 2013-2014, no consistent trends have been found for GEM or oxidized Hg over the six years or among the sites (Fig. SI-5 in Sect.

3 of SI). The interannual changes ranged from -1.8% to +3.9% for the annual average of GEM and from -13.3% to +28.6% for the annual average of GOM+PBM over 2009-2014.

Estimated mercury fluxes

At each monitoring site considered here, the calculated land cover-specific multi-hourly dry deposition fluxes of GEM, GOM and PBM were aggregated into land-cover specific and site-specific monthly, seasonal and annual values. Site-specific values were generated using a land cover area-weighted approach within a 3 km radius circle of each site. Annual values are provided in Table SI-3 and their statistics are shown in Fig. SI-6 in Sect. 4 of the SI. The six-year average of the seasonal values over various land covers is provided in Fig. SI-7, and the monthly site-specific values are provided in Fig. SI-8. Cases with insufficient data coverage were not presented.

Among the six years with concentration data and the 12 sites having the land cover of "deciduous broadleaf forest" (Fig. 2a), the annual flux during any calendar year (a negative value represents a net GEM emission) ranged from -5.0 to 14.3 μg m^{-2} yr^{-1}, 0.1 to 4.7 μg m^{-2} yr^{-1}, and 0.3 to 1.4 μg m^{-2} yr^{-1} for GEM, GOM, and PBM, respectively. The multi-year mean flux ranged from 2.7 to 12.4 μg m^{-2} yr^{-1}, 0.2 to 4.0 μg m^{-2} yr^{-1}, and 0.3 to 1.0 μg m^{-2} yr^{-1} for GEM, GOM, and PBM, respectively, among the 12 sites. The multi-year mean total dry deposition (the sum of GEM, GOM and PBM) ranged from 5.1 to 14.3 μg m^{-2} yr^{-1}, to which GOM plus PBM contributed 6-47% (figure not shown). Similar ranges of values were found for the other forest types. For example, if considering all of the forest land cover types together (Fig. SI-6b, c, d, e), the multi-year mean dry deposition ranged from 2.7 to 23.8 μg m^{-2} yr^{-1}, 0.1 to 4.0 μg m^{-2} yr^{-1}, and 0.3 to 1.8 μg m^{-2} yr^{-1} for GEM, GOM, and PBM, respectively, among the 19 sites, with the total dry deposition ranging from 5.1 to 23.8 μg m^{-2} yr^{-1} to which GOM plus PBM contributed 4-47%.

For other vegetated land cover types (Fig. SI-6f, g, h, i, j), multi-year mean dry deposition ranged from 0.8 to 22.1, 0.1 to 2.8, and 0.2 to 0.9 μg m^{-2} yr^{-1} for GEM, GOM, and PBM, respectively, among the 20 sites, with the total dry deposition ranging from 2.6 to 20.8 μg m^{-2} yr^{-1} to which GOM plus PBM contributed 2-69%. For urban and built-up land cover (Fig. SI-6 k), multi-year mean flux ranged from -1.4 to 10.0, 0.2 to 5.3, and 0.3 to 1.1 μg m^{-2} yr^{-1}, respectively, among the 10 sites, with the total dry deposition ranging from 2.4 to 11.2 μg m^{-2} yr^{-1} to which GOM plus PBM contributed 5-100%. Very limited data are available for the five sites having the water surface category (Fig. SI-6a), and these data showed annual GEM fluxes of 0.8 to 1.9 μg m^{-2} yr^{-1}, and GOM plus PBM fluxes of 0.2 to 1.3 μg m^{-2} yr^{-1} at four sites and 27.6 μg m^{-2} yr^{-1} at the elevated site (HI00) where extremely high oxidized mercury concentrations were recorded as shown in Fig. SI-3. Total dry deposition to water surfaces ranged from 1.0 to 3.2 μg m^{-2} yr^{-1} among the four non-elevated sites.

Comparing fluxes to different land covers within each site, it has been found that GEM had the highest deposition over forests due to large LAI values and the lowest deposition over urban and water surfaces due to high emission potentials and/or small LAI values. GOM and PBM also had high deposition over land covers with large LAI, but the differences in the deposition fluxes between different land covers were not as large as for GEM.

Seasonal average GEM deposition fluxes were the highest in winter and spring and the lowest (or emission at some sites) in summer over forests and several other vegetated land covers

(Fig. 2b and Fig. SI-7). Such a seasonal pattern can be explained by high GEM concentrations in the spring and winter (Fig. SI-4) and high GEM emissions in the summer due to high temperature. Seasonal average fluxes of the oxidized mercury did not show a consistent pattern from site to site or between different land covers; however, the highest seasonal fluxes were mostly observed in the spring, mainly due to the high GOM concentrations in this season (Fig. SI-4), noting that GOM dry deposited much faster than PBM.

Looking at site-specific (land cover area-weighted) monthly fluxes at all of the sites with available data (Fig. SI-8), emission fluxes were observed in one or two of the hottest months at some sites and in up to four or five months from May to September at some other sites, the latter case was due to high soil emissions and/or sites surrounded by land cover with small LAI. Thus, at several sites (e.g., OK99, FL96, AL19, GA40, OH02, WV99, MD08) the net flux from the sum of GEM, GOM and PBM was emission instead of deposition in the hottest several months of the year (Fig. 3).

Site-specific multi-year mean dry deposition is shown in Fig. 4. The flux patterns at two sites, AL19 and HI00, differed significantly from the rest of the sites. AL19 (an urban site), a net emission of GEM flux was obtained with a multi-year mean of -1.4 μg m^{-2} yr^{-1}. At HI00 (an elevated rural site), the extremely high GOM and PBM concentrations led to about 20 times higher dry deposition of GOM and PBM at this site than at the other sites. There are also five sites with insufficient data coverage (PBM at UT96, GOM at OH52, both GOM and PBM at WV99 and NJ05, and all of GEM, GOM and PBM at PA13). Excluding these seven sites, the other sites resulted in a multi-year mean Hg dry deposition of 4.6-22.0 μg m^{-2} yr^{-1}, with GEM contributing 43-97% and GOM plus PBM, 3-57% (Fig. SI-9). Coarse PBM contributed 43%, based on an average of all available sites, to the total PBM deposition, noting its mass fraction was assumed to be 30%. However, fine and coarse PBM together only accounted for a small fraction of the total Hg dry deposition, e.g. 11-15% at three sites and less than 8% at the rest of the sites. In comparison, the contribution from GOM to Hg deposition was about 2.5 times that from PBM if averaging all of the sites. The relative contributions from speciated mercury were mainly affected by their partitioning in air concentrations, site categories (emissions from surface), dominant land covers, and meteorological conditions.

Comparing the estimated dry deposition with MDN monitored wet deposition (Table SI-4 in Sect. 4 of SI), it was found that dry and wet deposition are equally important on an annual basis and at the regional scale, with dry deposition slightly higher than wet deposition (11.3 versus 9.4 μg m^{-2} yr^{-1}, or 20% higher on average from all complete data sets). At any individual site or during any individual year, the annual dry/wet ratio ranged from 0.4 to 3.5. On a seasonal basis and at the regional scale, the dry/wet ratio was 2.4, 1.7, 0.1, and 1.6 during the winter, spring, summer, and fall, respectively. Thus, dry deposition dominated over wet deposition in all of the seasons except in the summer, since dry deposition was mostly balanced by GEM emissions during the summer.

Uncertainty analyses in the estimated fluxes

Uncertainties in dry deposition estimation are typically on the order of a factor of 2.0 for seasonal or annual averages of the highly-studied pollutants, such as inorganic sulphur and nitrogen species[19]. Uncertainties in mercury dry deposition estimation are expected to be larger than those of sulfur and nitrogen species due to the greater challenges in measuring and

modeling mercury dry deposition. Several different measures were used below to assess the reliability of the estimated speciated and total mercury dry deposition.

The first measure was to assess if GEM emission was underestimated (or if net GEM deposition was overestimated). This was done by comparing the estimated GEM emission from the current bi-directional air surface exchange model (Sect. 5 of SI) with those simulated in a mercury transport model previously used by Zhang et al.[9] The ratio of GEM emission from the current study to the previous study was larger than 1.0 at all of the available sites except at MD98/99 (0.87/0.96), suggesting that GEM emission from the current study was not underestimated, and thus that the net GEM dry deposition is not substantially overestimated, assuming the previously-estimated GEM emission was within a reasonable range.

The second measure was to compare the estimated Hg dry deposition with measured litterfall Hg at the regional scale; as was done in Zhang et al.[9] This comparison is based on the assumption that the litterfall Hg measurements likely represent the low end of Hg dry deposition, because dry deposition also includes the portion that was initially uptake by leaf surface and was then washed off and uptake by underlying soil surfaces[9,20]. As mentioned above, the multi-year mean (2009-2014) Hg dry deposition ranged from 5.1 to 14.3 μg m^{-2} yr^{-1} to deciduous broadleaf forests, and from 5.1 to 23.8 μg m^{-2} yr^{-1} to all forest types. Annual litterfall Hg (2007-2014) from predominantly deciduous forests at 15 sites in eastern U.S. ranged from 3.5 to 23.4 μg m^{-2} yr^{-1} (Table SI-6 in SI)[21]. The same ranges in the estimated Hg dry deposition as the litterfall Hg on the regional scale suggest the reliability of the numbers, although with large uncertainties. Only five collocated sites (OH02, MD08, MD98/99, NY20, and VT99) had enough data for comparison between estimated Hg dry deposition and litterfall Hg over deciduous broadleaf forests, with the former in the range of 5.1 to 12.8 μg m^{-2} yr^{-1}, and the latter in the range of 11.3 to 18.8 μg m^{-2} yr^{-1}. This suggests that the results from the present study are likely conservative estimates.

Model estimates of GOM dry deposition discussed above seemed to be smaller by a factor of 2.0 or more when compared with some surrogate surface measurements[22], although they are close to others as discussed in Zhang et al.[9] Considering the large uncertainties and potential underestimation of the GOM concentrations measured by the Tekran instruments[14,23], a third measure was to increase the GOM concentration by a factor of 3.0, as was done in Huang and Gustin[24], to reassess the above conclusions. Note that coarse PBM has already been considered in the dry deposition budget so no further adjustment was made for PBM. With increased GOM concentrations, the total dry deposition to deciduous broadleaf forest ranged from 8.0 to 19.0 μg m^{-2} yr^{-1} among all of the sites, and from 8.5 to 19.0 μg m^{-2} yr^{-1} among the four collocated sites. These adjusted numbers still compare well with the litterfall measurements, further demonstrating the reliable and conservative estimates of speciated and total Hg dry deposition presented in this study.

The relative contributions from oxidized and elemental Hg to the Hg dry deposition were also reassessed with the above-mentioned GOM adjustments. GOM plus PBM contributions to the total dry deposition increased slightly to 5-78% from the original 3-57% at the sites shown in Fig. SI-9. Note that even after the adjustments, only four sites (UT97, OH02, MD08, NY06) had GOM plus PBM contributions exceeding 50%. Thus, it is concluded that in the North American environment where annual mean oxidized mercury were typically at 10 pg m^{-3}, total mercury dry deposition over vegetated surfaces was mostly dominated by GEM.

However, in many Asian countries where oxidized mercury is at much (e.g., five to 10

times) higher levels, GOM and PBM may dominate the dry deposition budget due to the significantly higher GOM and PBM deposition and the considerably lower net GEM deposition. The latter can be caused by the higher Hg emission potentials as a result of the higher GOM and PBM dry and wet deposition. The elevated site (HI00) in the present study belonged to this category, where GOM plus PBM accounted for 92% of the Hg dry deposition (Fig. 4 and Fig. SI-9).

To further confirm this hypothesis, a sensitivity test was conducted by increasing leaf emission potentials by 25% and doubling soil emission potentials up to a value of 30 (see details in Sect. 7 of SI). As a result, the net GEM dry deposition was reduced by half at some sites and net deposition became net emission at a few other sites. This seems to agree with what was proposed by Wang et al.[25] in China. In this scenario, if GOM and PBM dry deposition are further adjusted up by five to ten times, then GOM and PBM definitely dominate the dry deposition budget.

The uncertainty assessments discussed above suggest that the dry deposition budget provided in this study is reliable, although with large uncertainties. Emission potential from leaf stomata causes the largest uncertainties among all the model parameters, and thus seasonal-dependant, besides LUC-dependant, emission potentials should be tested in future studies. It is concluded that at rural and remote locations and at the regional scale in the North American environment, GEM was the main contributor to the net Hg dry deposition over vegetated canopies.

Responses of mercury dry deposition to emission reduction

If anthropogenic Hg emissions continue declining in North America, air concentrations of oxidized Hg are expected to decline faster than that of GEM due to the global reservoir and long lifetime of GEM. Dry deposition of oxidized Hg and Hg wet deposition, the latter is mainly from precipitation scavenging of oxidized Hg, are expected to decline accordingly. However, net GEM dry deposition may not decrease as fast as oxidized Hg does, and an increase of net GEM dry deposition to vegetated surfaces is also possible considering soil Hg emission potential will be lower due to the lower input of Hg into soil through dry and wet deposition of oxidized Hg.

To confirm the above hypothesis, the MD08 site was studied in more detail since this site has speciated Hg concentration data since 2006 and massive Hg emission reductions from power plants were observed during 2009-2012[26]. At this site GOM declined by 75% from 2006 to 2015 while GEM only declined by 13% during the same period[26]. Annual Hg wet deposition averaged at 8.6 μg m^{-2} yr^{-1} during 2006-2008 and at 7.1 μg m^{-2} yr^{-1} during 2009-2014, or a 20% decrease likely due to the Hg emission reductions.

Dry deposition for the year 2006 and 2007, representing the case before emission reduction, was compared with that of 2013 and 2014, representing the case of after emission reduction. Note that the soil emission potential in the years 2006 and 2007 was assumed to be 20% higher than that used for 2009-2014 due to the higher dry and wet deposition input in earlier years (Table SI-7). While dry deposition of oxidized Hg reduced by more than 50% in 2013-2014 compared to 2006-2007, dry deposition of GEM only reduced by 6% over croplands and increased by more than 10% over deciduous forest. Thus, dry deposition over vegetated canopies will not follow the same pattern as emission reductions due to the dominant contribution from GEM. Quantifying dry deposition based on land cover type is thus needed to assess the potential

Hg impact on various ecosystems.

To provide a prediction of deposition budget in future years in response to additional Hg emission reductions, sensitivity tests were conducted. MS12 site is shown as an example since this site has appreciable deposition of oxidized Hg and six years of complete data, and covers various land types (Table SI-8). Note that many sites considered in this study already had very low deposition from oxidized Hg (Table SI-3). It can be seen that while dry deposition of oxidized Hg decreased with reduced air concentrations, GEM dry deposition decreased at a much slower rate, and increased slightly in certain years over forest canopies.

The role of GEM in the Hg dry deposition budget is thus expected to become more important with continued Hg emission reductions. It will take longer time than the Hg emission reduction process to realize the benefits of reduced Hg emissions on the Hg deposition budget and the associated ecological effects over vegetated canopies, although immediate benefits may be realized over water and non-vegetated surfaces. Continued monitoring of speciated Hg at different site categories such as those listed in AMNet will provide the data needed for evaluating the long-term benefits of Hg emission reductions.

Methods:

The dry deposition flux of GOM (F_{GOM}) is estimated as the product of its air concentration (C_{GOM}) monitored at AMNet and its dry deposition velocity (V_{dGOM}) calculated using the dry deposition scheme of Zhang et al.[27] with modifications described in Zhang et al.[9]

$$F_{GOM} = C_{GOM} * V_{dGOM} \qquad (1)$$

$$V_{dGOM} = \frac{1}{R_a + R_b + R_c} \qquad (2)$$

where R_a, R_b and R_c are aerodynamic, quasi-laminar, and canopy resistances, respectively, and depend on meteorology and land use category (LUC).

AMNet collects PBM in fine particles less than 2.5 microns in size ($PM_{2.5}$). PBM in particles larger than 2.5 μm constitute a significant fraction of total PBM mass[287-30], and contribute even a larger fraction to total PBM dry deposition[31]. Based on available measurements of PBM size distributions and fine/coarse PBM mass ratios in the above-mentioned literature, 30% of the total PBM mass is assumed to be coarse particles in order to estimate total PBM dry deposition flux (F_{PBM}) where only fine PBM concentrations are available from AMNet.

$$F_{PBM} = C_1 V_{d1} + C_2 V_{d2} = C_1 (V_{d1} + \frac{f}{1-f} V_{d2}) \qquad (3)$$

where C_1 and C_2 are mass concentrations of PBM in fine and coarse particles, respectively, and V_{d1} and V_{d2} are corresponding dry deposition velocities. f is the mass fraction of PBM in coarse particles (0.3).

V_{d1} and V_{d2} are calculated according to Zhang and He[10]:

$$V_{d1} = V_d(PM_{2.5}) = V_g(PM_{2.5}) + \frac{1}{R_a + 1/(a_1 u_*)} \qquad (4)$$

$$V_{d2} = V_d(PM_{2.5-10}) = V_g(PM_{2.5-10}) + \frac{1}{R_a + 1/V_{ds}(PM_{2.5-10})} \quad (5)$$

$$V_{ds}(PM_{2.5-10}) = (b_1 u_* + b_2 u_*^2 + b_3 u_*^3) e^{(c_1 u_* + c_2 u_*^2 + c_3 u_*^3)(\frac{LAI}{LAI_{max}} - 1)} \quad (6)$$

where V_g is the gravitational settling velocity, u_* is the friction velocity, LAI is the leaf are index of a canopy, and a_1, b_1, b_2, b_3, c_1, c_2 and c_3 are LUC-dependent empirical constants.

Dry deposition (or air-surface exchange) flux of GEM (F_{GEM}) is estimated using a newly-developed bi-directional air-surface exchange scheme[11], taking the monitored GEM concentration (C_{GEM}) as input (note that a downward flux or deposition is given a positive value here in order to be consistent with the above equations):

$$F_{GEM} = \frac{(C_{GEM} - \chi_c)}{R_a + R_b} \quad (7)$$

$$\chi_c = \left[\frac{\chi_a}{R_a + R_b} + \frac{\chi_{st}}{R_{st} + R_m} + \frac{\chi_g}{R_{ac} + R_g}\right]\left[\frac{1}{R_a + R_b} + \frac{1}{R_{st} + R_m} + \frac{1}{R_{ac} + R_g} + \frac{1}{R_{cut}}\right]^{-1} \quad (8)$$

where χ_c is a mid-variable representing the GEM concentration at the canopy top. R_m and R_{st} are the mesophyll and stomatal resistances (s m^{-1}), R_{cut} is the cuticle resistance (s m^{-1}), and R_{ac} and R_g are the in-canopy aerodynamic and soil resistances (s m^{-1}), respectively. These resistances are the same as those used in Zhang et al.[9]

The stomatal and ground surface compensation points, χ_{st} and χ_g (μg m^{-3}), needed in the above equation are calculated using:

$$\chi_{st}(\mu g/m^3) = \frac{8.9803\times10^9}{T_{st}} \times \Gamma_{st} \times exp\left(-\frac{8353.8}{T_{st}}\right) \times 8.2041 \quad (9)$$

$$\chi_g(\mu g/m^3) = \frac{8.9803\times10^9}{T_g} \times \Gamma_g \times exp\left(-\frac{8353.8}{T_g}\right) \times 8.2041 \quad (10)$$

where Γ_{st} and Γ_g are the emission potentials of stomata and soil, respectively, and are defined empirically for each LUC surrounding each site of interest, as detailed in Sect. 1 of Supplemental Information (SI). The resistance terms in the above equations are calculated in the same way as for GOM and are described in Zhang et al.[9]

Meteorological data used as input for calculating deposition are from the archived data produced by the Canadian weather forecast model at a horizontal grid resolution of 15 km by 15 km. Hourly meteorological data at the surface and the first model-layer, typically at 40-50 meters in height for model grids containing the measurement sites, are extracted from the archived data.

Acknowledgements: The NADP/AMNet is able to function only with the work of the site operators, and Principal Investigators.

Supporting Information Available

Additional data tables and figures are enclosed in the Supporting Information document.

Author contributions: L.Z. designed the study, analyzed the results, and wrote most of the paper; Z.W., I.C. and L.P.W. contributed to computer programing, data processing, and paper writing; and other coauthors collected and quality controlled the mercury concentration data and provided comments on the paper.

References

1. Selin, N. E., Jacob, D. J., Park, R. J., Yantosca, R. M., Strode, S., Jaegle, L., and Jaffe, D., 2007. Chemical cycling and deposition of atmospheric mercury: global constraints from observations. *J. Geophys. Res.*, 112 (D02308), doi:10.1029/2006JD007450.
2. Strode, S. A., Jaegle, L., Selin, N. E., Jacob, D. J., Park, R. J., Yantosca, R. M., Mason, R. P., and Slemr, F., 2007. Air-sea exchange in the global mercury cycle. *Global Biogeochemical Cycles*, 21 (GB1017), doi:10.1029/2006GB002766.
3. Gustin, M. S., Lindberg, S. E., and Weisberg, P.J., 2008. An update on the natural sources and sinks of atmospheric mercury. *Applied Geochemistry*, 23, 482-493.
4. Pirrone, N., Cinnirella, S., Feng, X., Finkelman, R.B., Friedli, H.R., Leaner, J., Mason, R., (...), Telmer, K., 2010. Global mercury emissions to the atmosphere from anthropogenic and natural sources. *Atmos. Chem. Phys.*, 10, 5951-5964.
5. Provencher, J.F., Mallory, M.L., Braune, B.M., Forbes, M.R., Gilchrist, H.G., 2014. Mercury and marine birds in Arctic Canada: Effects, current trends, and why we should be paying closer attention. *Environmental Reviews*, 22, 244-255.
6. Schartup, A.T., Balcom, P.H., Soerensen, A.L., Gosnell, K.J., Calder, R.S.D., Mason, R.P., Sunderland, E.M., St. Louis, V.L., 2015. Freshwater discharges drive high levels of methylmercury in Arctic marine biota. *Proceedings of the National Academy of Sciences of the United States of America*, 112 (38), 11789-11794.
7. Giang, A. and Selin, N. E., 2016. Benefits of mercury controls for the United States. *Proceedings of the National Academy of Sciences, 113*, 286-291.
8. Gay, D. A., Schmeltz, D., Prestbo, E., Olson, M., Sharac, T., and Tordon, R., 2013. The Atmospheric Mercury Network: measurement and initial examination of an ongoing atmospheric mercury record across North America. *Atmos. Chem. Phys.*, 13, 11339-11349.
9. Zhang, L., Blanchard P., Gay D.A., Prestbo E.M., Risch M.R., Johnson D., Narayan J., Zsolway R., Holsen T.M., Miller E.K., Castro M.S., Graydon J.A., St. Louis V.L., and Dalziel J., 2012. Estimation of speciated and total mercury dry deposition at monitoring locations in eastern and central North America. *Atmos. Chem. Phys*, 12, 4327-4340.
10. Zhang, L. and He Z., 2014. Technical Note: An empirical algorithm estimating dry deposition velocity of fine, coarse and giant particles. *Atmos. Chem. Phys.*, 14, 3729-3737.
11. Wright, L.P and Zhang L., 2015. An approach estimating bi-directional air-surface exchange for gaseous elemental mercury at AMNet sites. *J. Advan. Modeling Earth Sys*., 7, 35-49.
12. USEPA, 2015. Toxics Release Inventory (TRI) Explorer, 2009-2014 Dataset (Released October 2015) Internet Database, available

at: http://iaspub.epa.gov/triexplorer/tri_release.facility, last accessed 21 March 2016.
13. National Atmospheric Deposition Program (NADP), 2016. Atmospheric Mercury Network Data, Illinois State Water Survey, Champaign IL. http://nadp.isws.illinois.edu/amn/data.aspx
14. Gustin, M. S., Amos, H. M., Huang, J., Miller, M. B., and Heidecorn, K., 2015. Measuring and modeling mercury in the atmosphere: a critical review. *Atmos. Chem. Phys*., 15, 5697-5713.
15. Swartzendruber, P. C., Jaffe, D. A., Prestbo, E. M., Weiss-Penzias, P., Selin, N. E., Park, R., Jacob, D. J., Strode, S. and Jaeglé, L., 2006. Observations of reactive gaseous mercury in the free troposphere at the Mount Bachelor Observatory. *J. Geophys. Res. Atmospheres*, 111 (D24), doi: 10.1029/2006JD007415.
16. Faïn, X., Obrist, D., Hallar, A. G., Mccubbin, I., and Rahn, T., 2009. High levels of reactive gaseous mercury observed at a high elevation research laboratory in the Rocky Mountains. *Atmos. Chem. Phys*., 9, 8049-8060.
17. Weiss-Penzias, P., Gustin, M. S., and Lyman, S. N., 2009. Observations of speciated atmospheric mercury at three sites in Nevada: Evidence for a free tropospheric source of reactive gaseous mercury. *J. Geophys. Res. - Atmospheres*, 114 (D14), doi: 10.1029/2008JD011607.
18. Lyman, S. N. and Jaffe, D. A. (2012). Formation and fate of oxidized mercury in the upper troposphere and lower stratosphere. *Nature Geosci*., 5, 114-117.
19. Flechard, C.R., Nemitz E., Smith R.I., Fowler D., Vermeulen A.T., Bleeker A., Erisman J.W., Simpson D., Zhang L., Tang Y.S., and Sutton M.A., 2011. Dry deposition of reactive nitrogen to European ecosystems: a comparison of inferential models across the NitroEurope network. *Atmos. Chem. Phys.*, 11, 2703-2728.
20. Wright, L.P., Zhang L., and Marsik F.J., 2016. Overview of mercury dry deposition, litterfall, and throughfall studies. *Atmos. Chem. Phys. Discuss*., doi:10.5194/acp-2016-474.
21. Risch, M.R., DeWild, J.F., Krabbenhoft, D.P., Kolka, R.K., Zhang, L., 2012: Mercury in Litterfall at Selected National Atmospheric Deposition Program Mercury Deposition Network Sites in the Eastern United States, 2007-2009. *Environ. Pollu.*, 161, 284-290.
22. Wright G., Gustin M.S., Weiss-Penzias P., Miller M.B., 2014. Investigation of mercury deposition and potential sources at six sites from the Pacific Coast to the Great Basin, USA. Science of the Total Environment 470–471, 1099–1113.
23. Jaffe, D. A., S. Lyman, H. M. Amos, M. S. Gustin, J. Huang, N. E. Selin, L. Leonard, A. Ter Schure, R. P. Mason, R. Talbot, A. Rutter, B. Finley, L. Jaeglé, V. Shah, C. McClure, J. Ambrose, L. Gratz, S. Lindberg, P. Weiss-Penzias, G.-R. Sheu, D. Feddersen, M. Horvat, A. Dastoor, A. J. Hynes, H. Mao, J. E. Sonke, F. Slemr, J. A. Fisher, R. Ebinghaus, Y. Zhang, and G. Edwards, 2014. Progress on understanding atmospheric mercury hampered by uncertain measurements, *Environ. Sci. Techol.*, 48, 7204-7206.
24. Huang J. and Gustin M.S., 2015. Use of passive sampling methods and models to understand sources of mercury deposition to high elevation sites in the western United States. *Environ. Sci. Technol*., 49, 432−441.
25. Wang, X. Lin C.-J., Yuan W., Sommar J., Zhu W., and Feng X., 2016. Emission-dominated gas exchange of elemental mercury vapor over natural surfaces in China. *Atmos. Chem. Phys. Discuss*., doi:10.5194/acp-2016-314.
26. Castro, M. S. and Sherwell, J., 2015. Effectiveness of Emission Controls to Reduce the Atmospheric Concentrations of Mercury. *Environ. Sci. Technol.*, 49, 14000-14007.

27. Zhang, L., Brook J.R., and Vet R., 2003. A revised parameterization for gaseous dry deposition in air-quality models. *Atmos. Chem. Phys.*, 3, 2067-2082.
28. Pirrone, N., Keeler, G.J., Allegrini, I., 1996. Particle size distributions of atmospheric mercury in urban and rural areas. *J Aerosol Science*, 27 (SUPPL.1), S13-S14.
29. Feddersen, D.M., Taibot, R., Mao, H., Sive, B.C., 2012. Size distribution of particulate mercury in marine and coastal atmospheres. *Atmos. Chem. Phys.*, 12, 10899-10909.
30. Kim, P.-R., Han, Y.-J., Holsen, T.M., Yi, S.-M., 2012. Atmospheric particulate mercury: Concentrations and size distributions. *Atmos. Environ.*, 61, 94-102.
31. Fang, G.C., Zhang L., and Huang C.S., 2012. Measurements of size-fractionated concentration and bulk dry deposition of atmospheric particulate bound mercury. *Atmos. Environ.*, 61, 371-377.

List of Tables

List of Figures

Table 1. AMNet sites listed in order from the Pacific to Atlantic coast; symbols adjacent to the sites indicate collocated instruments. [a] Site categorization reported in Gay et al. (2013). [b] Percentage area of MODIS land cover within the 3 km radius circle is provided in parentheses. [c]Average annual Hg air emissions (kg) within 100 km radius. [d] Multi-year mean air concentration.

AMNet site ID	**Site name**	**Latitude, longitude**	**Data coverage**	**Site category[a]**	**Dominant land type within 3 km radius[b]**	**Hg emission[c]**	**GEM[d]** ($ng\ m^{-3}$)	**GOM** ($pg\ m^{-3}$)	**PBM** ($pg\ m^{-3}$)
CA48	Elkhorn Slough	36.8100, 121.780	Jan/2010-Dec/2011	Suburban	Water (26.4), Grasslands (19.3), Croplands (15.6), Urban and built up (14.1), Permanent wetlands (7.3), Closed shrublands (6.7), Woody savannas (6.1)	131	1.48	0.71	3.35
UT96	Antelope Island	41.0885, 112.119	Jun/2009-Jun/2011	Suburban	Croplands (58.9), Grasslands (26.5), Water (6.3)	233	1.65	11.7	na
UT97	Salt Lake City	40.7118, 111.961	Jan/2009-Dec/2014	Urban	Urban and built up (99.2)	108	1.93	20.4	16.1
OK99	Stilwell	35.7508, 94.6696	Jan/2009-Nov/2014	Rural	Grasslands (46.5), Woody savannas (33.6), Deciduous broadleaf forest (19.8)	472	1.31	2.26	4.31
WI07	Horicon	43.4557, 88.6169	Jan/2011-Dec/2014	Rural	Croplands (85.5), Urban and built up (8.3), Permanent wetlands (5.9)	355	1.46	1.93	8.52
*MS12	Grand Bay NERR	30.4124, 88.4038	Jan/2009-Dec/2014	Rural	Woody savannas (32.6), Permanent wetlands (27.4), Closed shrublands (11.7), Evergreen broadleaf forest (9.7), Evergreen needleleaf forest (9.5), Mixed forest (7.7)	384	1.40	5.55	6.99
*MS99							1.41	5.78	6.19
FL96	Pensacola	30.5500, 87.3753	Jan/2009-Dec/2014	Rural	Woody savannas (49.1) , Grasslands (17.3), Croplands (14.3), Evergreen broadleaf forest (13.3), Evergreen needleleaf forest (5.7)	304	1.36	1.61	3.13
AL19	Birmingham	33.5530, 86.8148	Jan/2009-Dec/2014	Urban	Urban and built up (99.2)	1096	1.98	19.3	9.56
GA40	Yorkville	33.9283, 85.0456	Jan/2009-Dec/2014	Rural	Woody savannas (49.3), Mixed forest (40.2), Deciduous broadleaf forest (10.5)	294	1.36	2.89	5.11
OH52	South Bass Island	41.6582, 82.8272	Jan/2013-Dec/2014	Rural	Water (67.1), Permanent wetlands (13.2), Grasslands (9.9), Mixed forest (6.2)	718	1.80	7.89	8.75
OH02	Athens	39.3080, 82.1182	Jan/2009-Dec/2014	Rural	Deciduous broadleaf forest (45.3), Croplands (25.1), Grasslands (21.2), Urban and built up (8.4)	1210	1.42	7.74	9.89
WV99	Canaan Valley Institute	39.1189, 79.4522	Jan/2009-Oct/2012	Rural	Deciduous broadleaf forest (54.7), Mixed forest (26.2), Grasslands (19.1)	583	1.28	2.94	2.76
MD08	Piney Reservoir	39.7054, 79.0126	Jan/2009-Dec/2014	Rural	Deciduous broadleaf forest (50.5), Croplands (49.5)	1114	1.36	8.89	7.25
PA13	Allegheny Portage	40.4571, 78.5603	Nov/2009-Sep/2011	Rural	Deciduous broadleaf forest (73.5), Croplands (14.0), Grasslands (11.0)	863	1.42	5.24	0.43
§NY43	Rochester	43.1463, 77.5483	Jan/2009-Dec/2014	Suburban	Urban and built up (63.6), Grasslands (16.7), Woody savannas (8.5), Deciduous broadleaf forest (7.1)	85	1.45	4.40	12.5
§NY95							1.58	4.73	6.85
ǂMD98	Beltsville	39.0283,	Jan/2009-	Rural	Mixed forest (44.3), Croplands (41.5), Deciduous	217	1.40	4.76	8.05

AMNet site ID	Site name	Latitude, longitude	Data coverage	Site category[a]	Dominant land type within 3 km radius[b]	Hg emission[c]	GEM[d] ($ng\ m^{-3}$)	GOM ($pg\ m^{-3}$)	PBM ($pg\ m^{-3}$)
ǂMD99		76.8171	Dec/2014		broadleaf forest (12.3)		1.41	3.54	8.45
NJ05	Brigantine	39.4649, 74.4488	Jun/2009-Apr/2010	Suburban	Mixed forest (26.9), Water (17.7), Evergreen needleleaf forest (13.1), Croplands (12.4), Woody savannas (12.4), Permanent wetlands (10.7)	80	1.45	1.18	5.48
NY20	Huntington Wildlife Forest	43.9736, 74.2232	Jan/2009-Dec/2014	Rural	Mixed forest (58.8), Deciduous broadleaf forest (40.0)	13	1.28	0.87	6.84
NY06	NYC	40.8679, 73.8782	Jan/2009-Dec/2014	Urban	Urban and built up (100)	71	1.63	6.40	8.86
VT99	Underhill	44.5285, 72.8682	Jan/2009-Dec/2014	Rural	Deciduous broadleaf forest (71.1), Mixed forest (28.9)	2	1.36	1.57	7.95
NH06	Thompson Farm	43.1088, 70.9485	Jan/2009-Nov/2011	Rural	Mixed forest (75.8), Deciduous broadleaf forest (9.7), Urban and built up (7.7), Croplands (6.8)	46	1.34	2.34	3.67
ME97	Presque Isle	46.6964, 68.0332	Dec/2013-Dec/2014	Suburban	Croplands (69.3), Mixed forest (22.9), Urban and built up (7.6)	5	1.57	2.35	4.58
NS01	Kejimkujik National Park	44.4321, 65.2031	Jan/2009-Dec/2014	Rural	Mixed forest (98.3)	0	1.33	0.36	5.09
HI00	Mauna Loa	19.5362, 155.576	Jan/2011-Dec/2014	Rural	Barren or sparsely vegetated (93.8), Water (6.2)	14	1.39	147	68.2

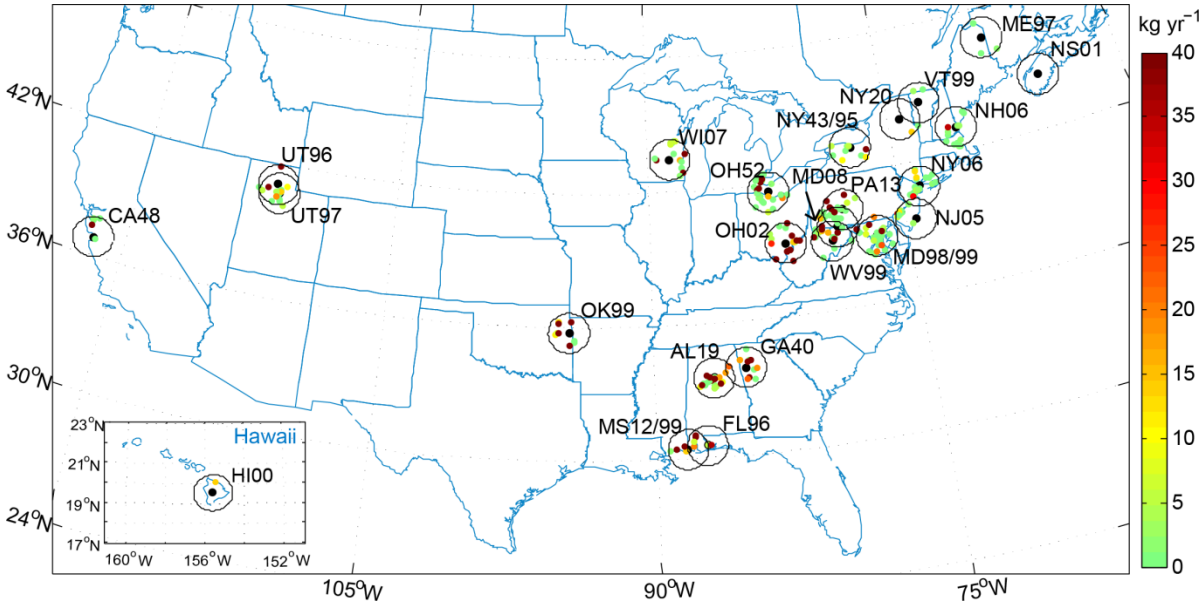

Figure 1. Map of AMNet sites and mercury air emission sources within a 100 km radius.

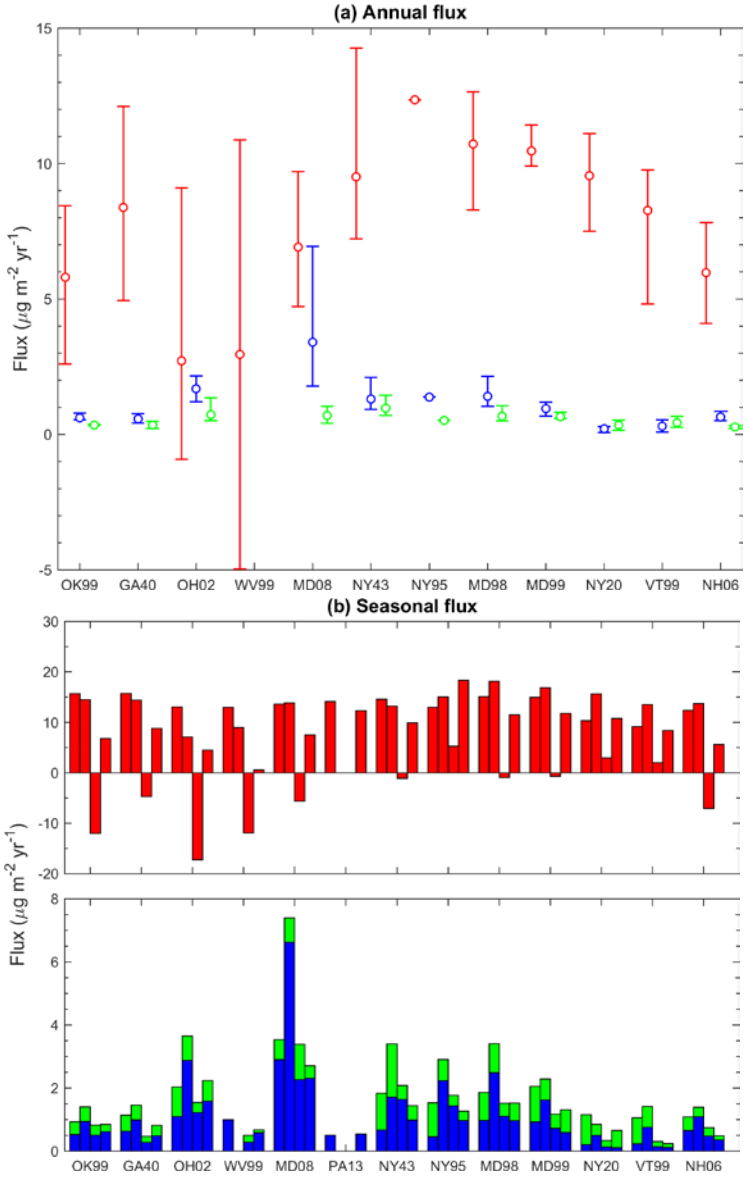

Figure 2. Estimated speciated mercury (GEM-red, GOM-blue, and PBM-green) fluxes over deciduous broadleaf forests. (a) Mean (circle) and range (vertical line) of the annual values between 2009-2014; and (b) six-year average of seasonal values (four columns at each site represent winter, spring, summer, and autumn, respectively). Only sites having the specific land cover within a 3-km radius circle are shown and sites are arranged in order from the Pacific to Atlantic coast.

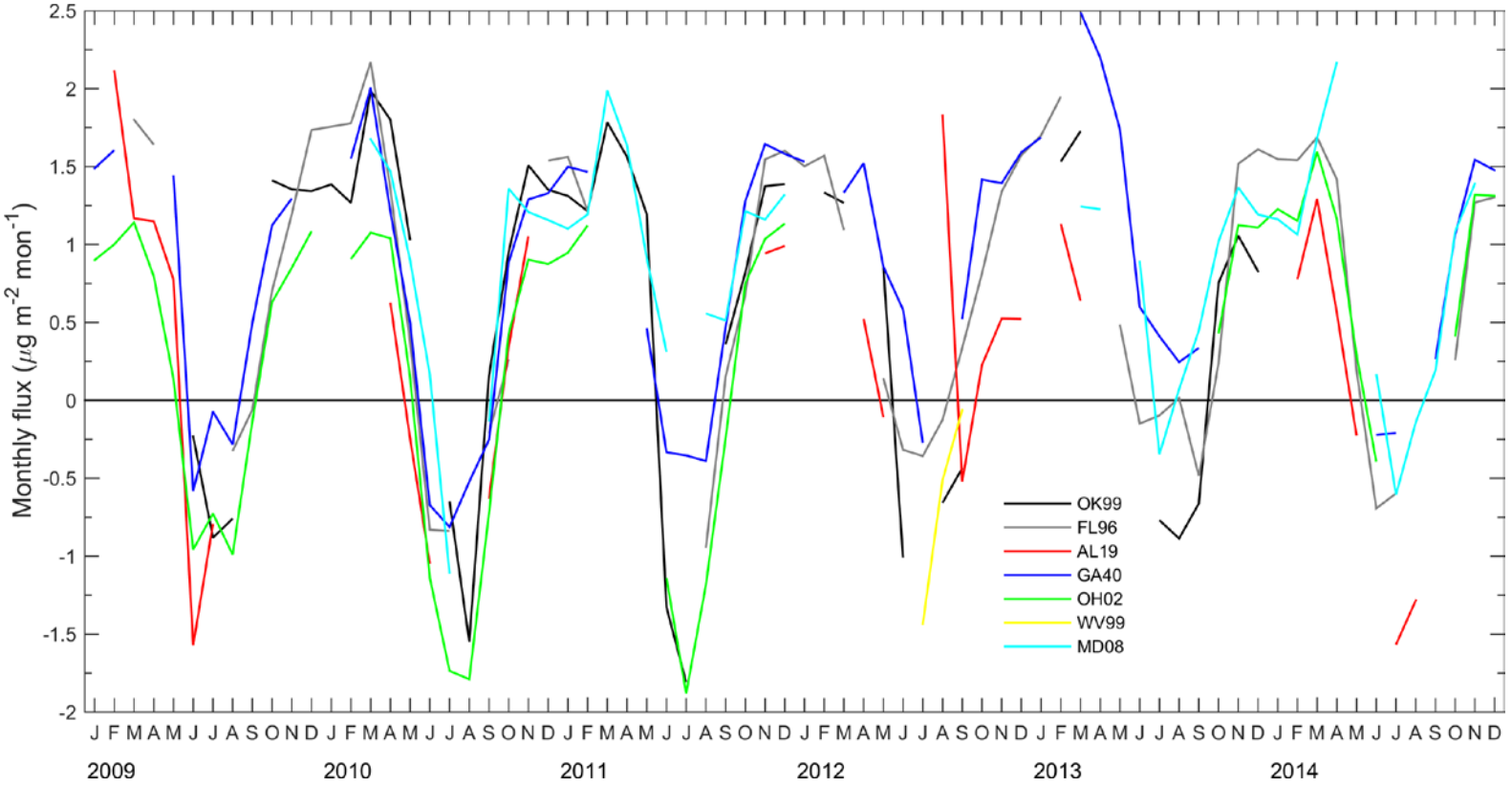

Figure 3. Time series of monthly land cover area-weighted mercury fluxes from 2009-2014 at selected sites.

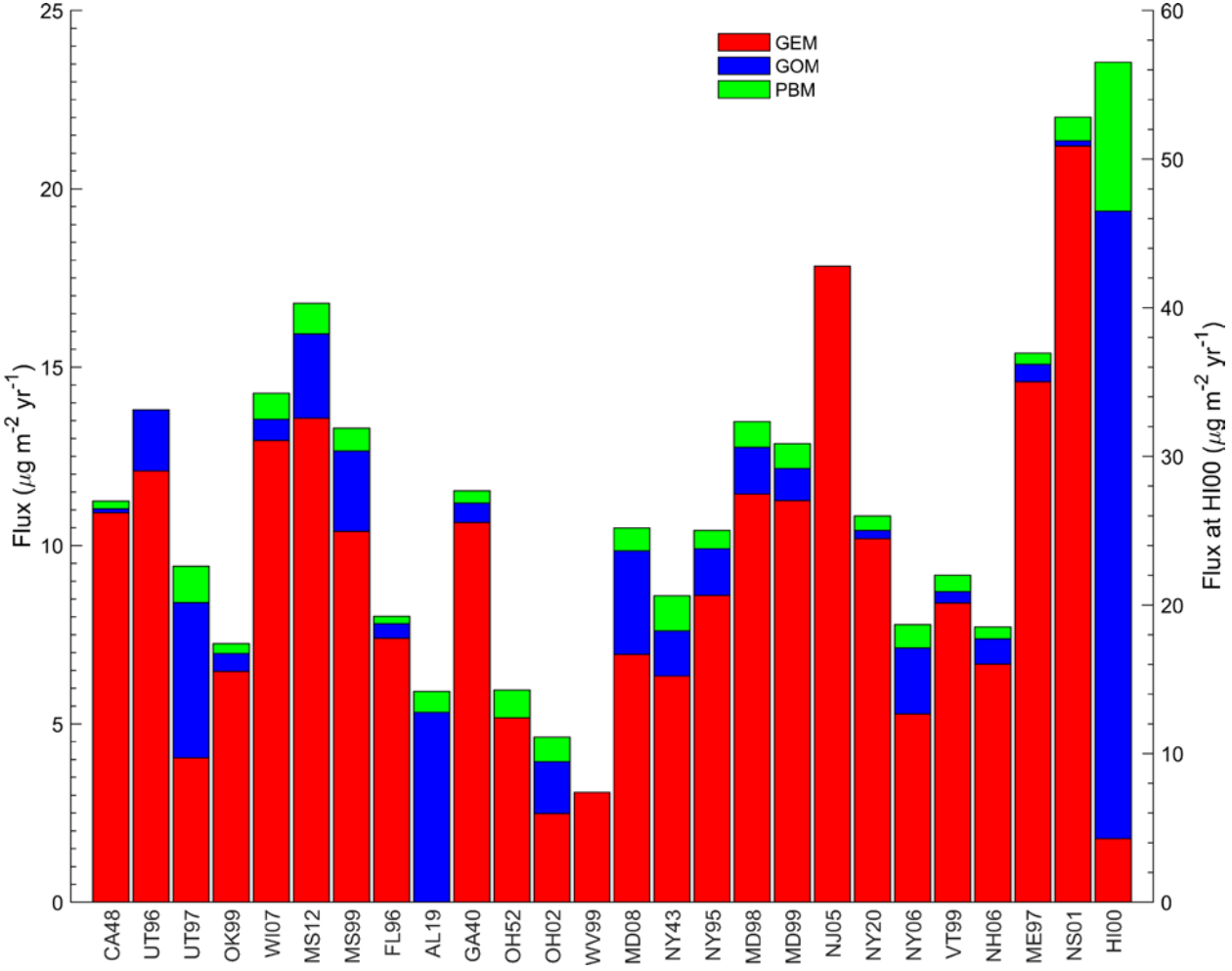

Figure 4. Multi-year mean land cover area-weighted dry deposition at all of the sites. Note the insufficient data coverage of PBM at UT96, GOM at OH52, and both GOM and PBM at WV99 and NJ05.